Journal of Magnetic Resonance 204 (2010) 82–90

Contents lists available at ScienceDirect

Journal of Magnetic Resonance

journal homepage: www.elsevier.com/locate/jmr

Ultrafast 2D COSY with constant-time phase-modulated spatial encoding

Can Wu, Mingfang Zhao, Shuhui Cai *, Yulan Lin, Zhong Chen

Department of Physics, Fujian Key Laboratory of Plasma and Magnetic Resonance, State Key Laboratory of Physical Chemistry of Solid Surfaces, Xiamen University, Xiamen 361005, China

ARTICLE INFO

Article history:
Received 31 October 2009
Revised 2 February 2010
Available online 12 February 2010

Keywords:
Ultrafast 2D NMR
^{1}H NMR
2D g-COSY
2D gDQF-COSY
Spatial encoding

ABSTRACT

Recently ultrafast techniques enable 2D NMR spectra to be obtained in a single scan. They have been successfully applied for 2D COSY, TOCSY, DOSY, HMQC and *J*-resolved spectra. In this paper, two alternative ultrafast 2D COSY methods (g-COSY and gDQF-COSY) based on continuous constant-time phase-modulated spatial encoding were proposed. Theoretical expressions of the resulting signals were deduced. Experiments were performed to verify our theoretical analysis and the feasibility of the methods. Comparisons between the experimental results from our methods and the previous real-time phase-modulated spatial encoding method demonstrate that the signal-to-noise ratio and resolution of the 2D COSY spectra are improved and a good 2D COSY spectrum is easier to achieve by using our methods.

1. Introduction

Nuclear magnetic resonance (NMR) plays a significant role in determining structures and dynamics of various physical, chemical and biological systems at molecular level [1]. The introduction of two-dimensional (2D) techniques accelerates and extends the application of NMR spectroscopy [2,3]. 2D NMR spectroscopy fulfills a central role in the application of NMR on chemistry, biology and medicine. 2D NMR spectroscopy separates and correlates spin interactions along two independent frequency domains, resulting in an enhancement in resolution and information that is unavailable in unidimensional counterpart. One of the typical 2D NMR experiments is homonuclear correlation spectroscopy (COSY), which serves as a powerful tool for analyzing complex proton NMR spectra. The pulse sequence of COSY is composed of two $\pi/2$ radio-frequency (RF) pulses. Generally, a 2D COSY spectrum consists of diagonal peaks and cross peaks. The diagonal peaks represent the inequivalent nuclei, and the cross peaks indicate the existence of *J*-coupling between the related nuclei. The first COSY experiment was performed over 30 years ago [3]. The pulse sequence, $(\pi/2)$–t_1–$(\pi/2)$–t_2, gives rise to a phase-modulated signal which allows, after 2D Fourier transform (FT), to obtain chemical shift and *J*-coupling information in 2D NMR spectra. Unfortunately, numerous t_1 increments have to be collected for a spectrum with good resolution, which leads the experiment fairly time-consuming.

Conventional 2D COSY spectra are often displayed in a magnitude (or absolute value) mode due to different lineshape of diagonal and cross peaks, which means the loss of spectral phase information and the reduction of spectral resolution. This shortage is overcome by 2D double-quantum filtered COSY (DQF-COSY) which allows us to retrieve the phase information from the phase-sensitive signals [4–6]. A DQF-COSY spectrum can be phase corrected to pure absorptive diagonal and cross peaks in both direct and indirect dimension. This results in higher resolution than magnitude displayed counterpart. Moreover, the strong signals which do not experience homonuclear *J*-coupling are eliminated in the DQF-COSY spectra, which benefits for solvent suppression. Although 2D DQF-COSY takes these advantages, it is bothered by long experimental time in practical application as conventional 2D COSY.

Accelerating the speed of 2D NMR acquisition is an important research topic in NMR community. Plenty of software-based methods have been designed to obtain 2D NMR spectra as quickly as possible. For example, Schanda and Brutscher optimized the delays and pulse flip angles in heteronuclear multiple quantum coherence (HMQC) sequence (SOFAST-HMQC) to obtain 2D spectra of protein samples in a few seconds [7]. Some unconventional sampling schemes were also proposed, such as radial sampling and concentric ring sampling [8–11]. Based on the acquisition of a small number of t_1 increments, the methods of linear prediction (LP) [12,13], maximum entropy (Max-Ent) [13,14] and projection reconstruction (PR) [15] were applied to construct the whole 2D FID signals. In addition, alternative strategies to FT NMR were suggested, such as filter diagonalization method (FDM) [16] and Hadamard spectroscopy [17,18]. All these strategies effectively shorten the duration of indirect dimension; however, repetition of several transients is still required.

* Corresponding author. Fax: +86 592 2189426.
E-mail address: shcai@xmu.edu.cn (S. Cai).

1090-7807/$ - see front matter © 2010 Elsevier Inc. All rights reserved.
doi:10.1016/j.jmr.2010.02.005

Recently, a novel method based on ultrafast imaging technique was proposed by Frydman and coworkers, enabling the acquisition of a 2D NMR spectrum within a single scan [19,20]. In this so-called "ultrafast 2D NMR" technique, the usual t_1 encoding is replaced by a spatial encoding, which is decoded during the detection period by an echo planar imaging (EPI) detection scheme. However, the discrete encoding mode initially proposed suffers from some practical drawbacks as it requires fast gradient switching which must be carefully synchronized with RF irradiation. Moreover, it leads to the appearance of undesirable "ghost peaks" in the indirect dimension [21]. To deal with these limitations, Pelupessy introduced adiabatic pulses into the excitation scheme of this ultrafast method [22]. Shrot et al. then put forward a continuous encoding scheme using a pair of $\pi/2$ chirped pulses together with a pair of bipolar gradients [23]. Unfortunately, this method involves an amplitude modulation which is incompatible with the phase-modulated COSY.

Alternatives were worked out in succession to obtain phase-modulated encoding, including real-time and constant-time phase-modulated encodings [22,24–27]. These phase-modulated encoding techniques provide the opportunity to achieve ultrafast COSY spectra. Tal et al. pointed out that a real-time phase-modulated encoding with a $\pi/2$–π chirped pulse scheme could give a 2D COSY spectrum within about 100 ms [24]. However, this technique requires careful parameter calibration and it is not easy to implement in routine procedures. In this paper, an alternative method based on the constant-time phase-modulated encoding with a π–π chirped pulse scheme is proposed to obtain 2D g-COSY spectra. The principle of this method is derived and experimental examples are illustrated. A comparison between this method and the real-time phase-modulated encoding method [24] is given in terms of spectral resolution and signal-to-noise ratio (SNR). In view of the above-mentioned advantages of 2D DQF-COSY, we also introduce the ultrafast acquisition technique into 2D gDQF-COSY. The same constant-time phase-modulated encoding module is used as ultrafast 2D g-COSY pulse sequence. Experiments are performed to valuate its feasibility.

2. Theoretical formalism

Single-scan ultrafast NMR scheme was initially proposed by Frydman and coworkers, which was realized with the help of a discrete encoding module during the encoding period and an EPI detection block during the decoding period [19,20]. Although some limitations, such as some practical drawbacks and annoying "ghost peaks", exist in this scheme, its basic principle is still important for understanding other ultrafast NMR methods. The discrete encoding single-scan ultrafast 2D NMR sequence is depicted in Fig. 1a. It consists of a discrete encoding module ((i) of Fig. 1a) and an EPI detection block ((ii) of Fig. 1a). In the discrete encoding module, a discrete train of N_1 RF pulses are applied at a constant frequency increment $\Delta O = |O_{j+1} - O_j|$ ($j = 1, 2, \ldots, N_1$) and spaced by a constant delay Δt_1. Each excitation pulse is applied in combination with a pair of bipolar z-orientation field gradients (G_e and $-G_e$). This module effectively partitions the sample into N_1 independent spin packets positioned at specific z_j coordinates, whose evolution phases become encoded along z-orientation according to $\varphi(z_j) = C\Omega_1(z_j - z_{N1})$, where $C \approx 2\gamma G_e \Delta t_1/\Delta O$, Ω_1 is the internal frequency shift of spins during the encoding period, γ is the gyromagnetic ratio. In the EPI detection block, the evolution phases at different coordinates are decoded with the help of a pair of bipolar z-orientation field gradients (G_a and $-G_a$). The EPI detection block is repeated N_2 times.

In the end of the pulse sequence, spins become specifically decoded according to their spatial positions as well as their internal evolution frequencies. Such process can be summarized by an evolution phase

$$\phi(z) = \varphi(z) + {}_2t_2 + z \cdot \int_0^{t_2} \gamma G_a(t)dt, \qquad (1)$$

where $\varphi(z) = \Omega_1 t_1(z) = C\Omega_1(z - z_{N1})$; Ω_2 is the internal frequency shift of spins during the decoding period; t_2 is the acquisition time. Using $F(t_1, t_2)$ and $P(\Omega_1, \Omega_2)$ to describe the time-domain and frequency-domain signals, respectively, the relation of $F(t_1, t_2)$ and $P(\Omega_1, \Omega_2)$ can be summarized as

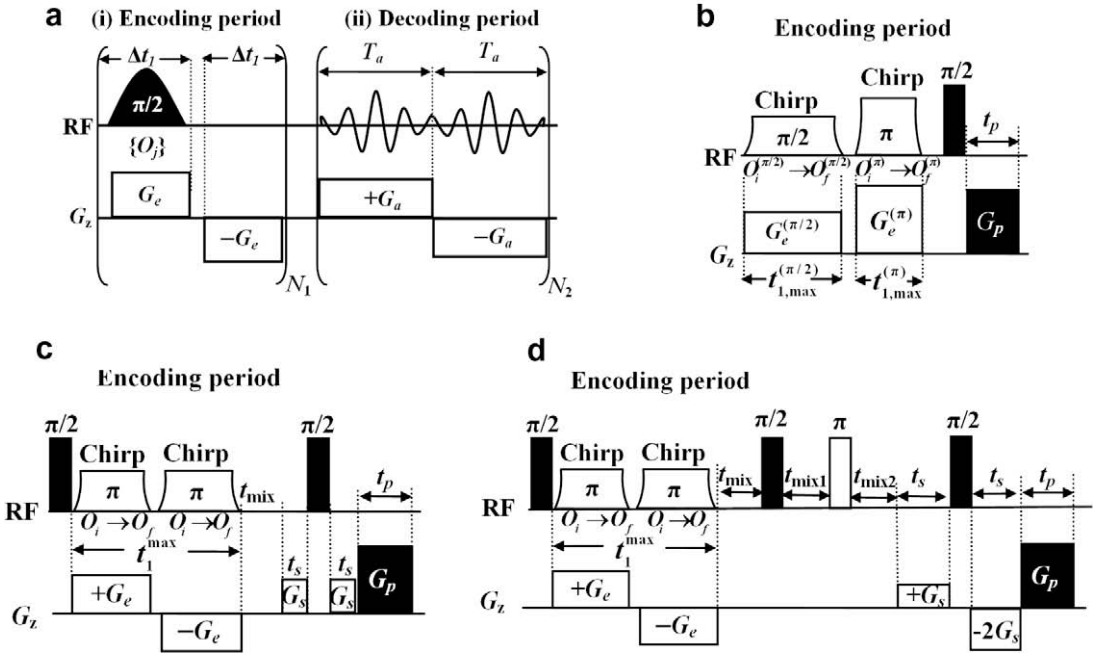

Fig. 1. (a) Discrete encoding single-scan ultrafast 2D NMR sequence [20], (b) continuous real-time phase-modulated encoding module for ultrafast 2D COSY [24], (c) constant-time phase-modulated encoding module [22] for ultrafast 2D g-COSY and (d) constant-time phase-modulated encoding module [22] for ultrafast 2D gDQF-COSY.

$$F(t_1,t_2)=\int_{\Omega_1}\int_{\Omega_2}\int_z P(\Omega_1,\Omega_2)e^{i\phi}d\Omega_1\,d\Omega_2\,dz. \quad (2)$$

According to Eq. (1), $e^{i\phi}$ can be described as $e^{i[\Omega_1 t_1(z)+\Omega_2 t_2+z\cdot\int_0^{t_2}\gamma G_a(t)dt]}$. Suppose that k is a gradient-related wave number encoding position, and $k=\int_0^{t_2}\gamma G_a(t)dt$. In the hybrid k space with k and t_2 variables, the signal can be described as

$$F(k,t_2)=\int_{\Omega_1}\int_{\Omega_2}\int_z P(\Omega_1,\Omega_2)e^{i(\Omega_1 t_1(z)+\Omega_2 t_2+kz)}d\Omega_1\,d\Omega_2\,dz. \quad (3)$$

Assume that $F(z,t_2)=\int_{\Omega_1}\int_{\Omega_2}P(\Omega_1,\Omega_2)e^{i\Omega_1 t_1(z)}e^{i\Omega_2 t_2}d\Omega_1 d\Omega_2$, Eq. (3) can be simplified as

$$F(k,t_2)=\int_z F(z,t_2)e^{ikz}dz. \quad (4)$$

Eq. (4) indicates that when the signal $F(k,t_2)$ in the k space is obtained, an FT of $F(k,t_2)$ can rebuild the signal $F(z,t_2)$. Since $F(z,t_2)=\int_{\Omega_1}\int_{\Omega_2}P(\Omega_1,\Omega_2)e^{i\Omega_1 t_1(z)}e^{i\Omega_2 t_2}d\Omega_1 d\Omega_2$, a 2D FT of $F(z,t_2)$ can thus provide a 2D NMR spectrum $P(\Omega_1,\Omega_2)$. Actually, a 1D FT of $F(k,t_2)$ along the t_2 dimension can directly provide the 2D NMR spectrum $P(\Omega_1,\Omega_2)$.

The above single-scan ultrafast NMR scheme enables us to obtain a 2D ^{1}H–^{1}H COSY spectrum within much shorter time than traditional 2D COSY method [20]. However, the discrete encoding mode requires fast gradient switching carefully synchronized with RF irradiation. Moreover, annoying "ghost peaks" will appear in the indirect dimension. To circumvent these limitations, a continuous real-time phase-modulated encoding mode with a $\pi/2$–π chirped pulse scheme replacing the discrete encoding scheme was proposed (Fig. 1b) [24]. The $\pi/2$ chirped pulse sweeps from initial frequency offset $O_i^{(\pi/2)}$ to final frequency offset $O_f^{(\pi/2)}$, and the π chirped pulse sweeps from $O_i^{(\pi)}$ to $O_f^{(\pi)}$. Different gradients ($G_e^{(\pi/2)}$, $G_e^{(\pi)}$) over unequal times ($t_{1,\max}^{(\pi/2)}$, $t_{1,\max}^{(\pi)}$) during the course of encoding are used. The conditions $G_e^{(\pi/2)}t_{1,\max}^{(\pi/2)}=2G_e^{(\pi)}t_{1,\max}^{(\pi)}$ and $G_e^{(\pi)}\approx 10G_e^{(\pi/2)}$ are chosen for the indirect-dimension encoding. A $\pi/2$ hard pulse and a purge period with a z-orientation field gradient (G_p) over a carefully calibrated time are applied after the encoding module. The same EPI detection block as in Fig. 1a is applied at the end of the sequence. The shortage of continuous real-time phase-modulated encoding sequence is that the parameters in this sequence must be carefully calibrated to make the spectral resolution and SNR acceptable.

In this paper, we propose an alternative ultrafast pulse sequence for the acquisition of 2D COSY spectra, which is based on the constant-time phase-modulated encoding [22,24,25,27]. A π–π chirped pulse scheme is used to replace the $\pi/2$–π chirped pulse scheme, as shown in Fig. 1c. For the π chirped pulses, the RF sweeps from initial frequency offset O_i to final frequency offset O_f at a constant rate $R=2\gamma G_e L/t_1^{\max}$, where L is the effective length of RF excitation and $t_1^{\max}$ is the total duration of the two π pulses. A pair of bipolar z-orientation field gradients ($+G_e$, $-G_e$) over equal time during the course of encoding are used. Two $\pi/2$ hard pulses are, respectively, imposed before and after the π–π module. A pair of z-orientation field gradients with the same duration (t_s) and strength (G_s) flank the second $\pi/2$ hard pulse to select the desired coherence order. The coherence-transfer pathway is shown at the bottom of Fig. 2a. Alternatively, the desired coherence order could also be selected by the same pair of field gradients applied after the first and the last $\pi/2$ hard pulse, respectively [28]. It is worth mentioning that two ways are available to shift the peaks in the indirect dimension for this pulse sequence. As usual, a z-orientation

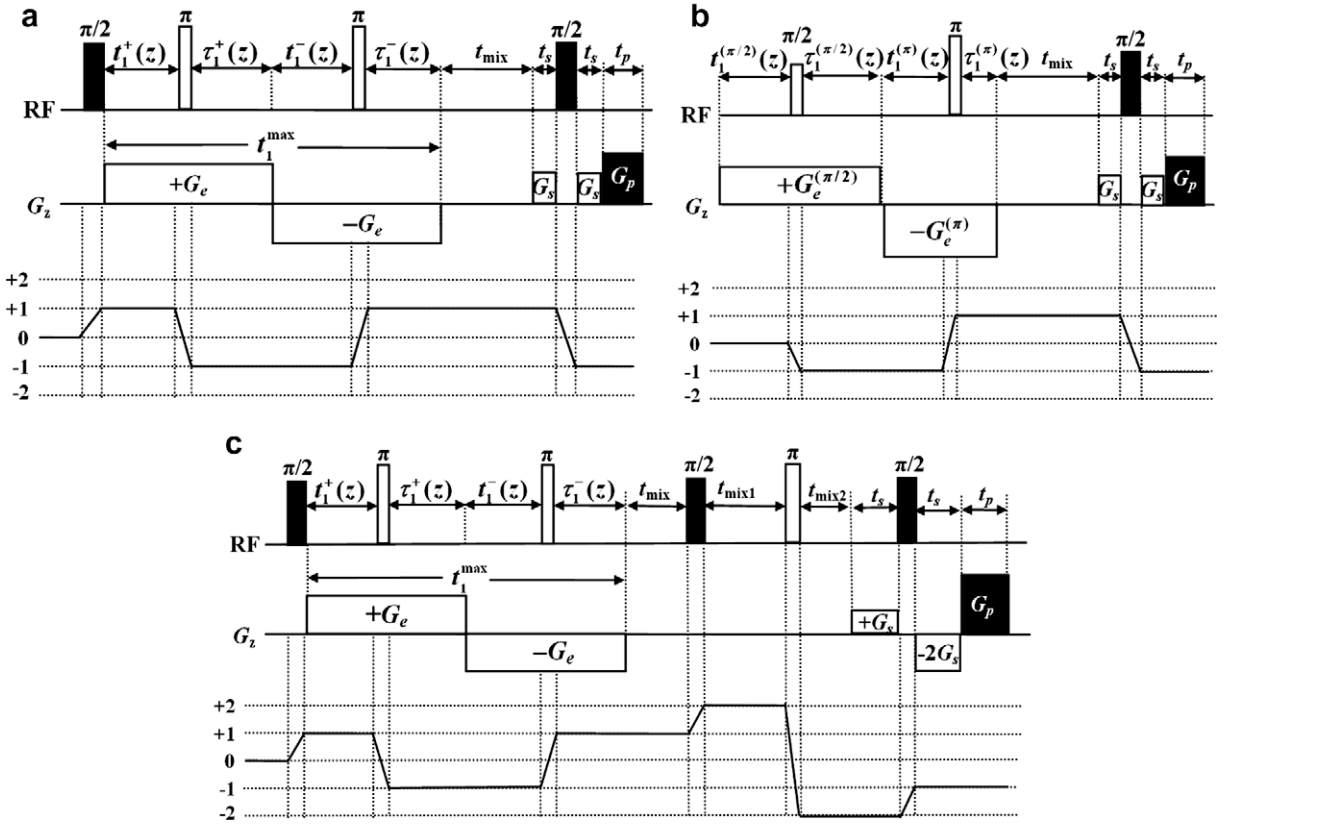

Fig. 2. Approximation of the phase-modulated encoding module of Fig. 1 acting on the spin packet at position z. (a) Encoding module of Fig. 1c, (b) encoding module of Fig. 1b in combination with a pair of pulse field gradients for coherence selection, and (c) encoding module of Fig. 1d. The related coherence-transfer pathways are given at the bottom of the pulse sequences.

field gradient (G_p) is effective to localize the peaks in the indirect dimension. This can also be achieved by adjusting the frequency offsets for observe transmitter of two π–π chirped pulses. The same EPI detection block as in Fig. 1a is used in the decoding period.

Suppose that the pulse sequence composed of the phase-modulated encoding module of Fig. 1c and the EPI detection block is applied to a sample of an AX spin-1/2 system, A and X represent I and S spins with internal frequency shifts Ω_I and Ω_S, and a scalar coupling constant J_{IS}. The effective length of the sample is L (the z coordinate ranges from $-L/2$ to $L/2$). All the RF pulses are applied along the x direction. Ignoring the effects of diffusion, relaxation and radiation damping, we will see how the spins evolve under the pulse sequence. Since the final signal is directly related to the evolution of spins, we start our theoretical deduction from reduced density operator. For the AX spin system discussed herein, the reduced density operator σ_{eq} for the two protons in each molecule at initial thermal equilibrium state with the high-temperature approximation can be given by

$$\sigma_{eq} = I_z + S_z, \tag{5}$$

where the Boltzmann factor has been omitted for clarity. I_z and S_z represent the longitudinal components of I and S spins, respectively. Since S is similar to I in an AX spin-1/2 system, only I is considered in the following deduction.

Due to the existence of the field gradients $\pm G_e$, the π chirped pulses sequentially excite the sample layer by layer along the z-axis. The action of pulse sequence on the spin packet at position z can be represented as Fig. 2a. The evolution time of spin packet at position z after the first $\pi/2$ pulse can be approximated to

$$\begin{aligned} t_1^+(z) &= \frac{\Omega_I + \gamma G_e z - O_i}{R}, \quad \tau_1^+(z) = \frac{t_1^{\max}}{2} - t_1^+(z) = \frac{O_f - \gamma G_e z - \Omega_I}{R}, \\ t_1^-(z) &= \frac{-O_i - \gamma G_e z + \Omega_I}{R}, \quad \tau_1^-(z) = \frac{t_1^{\max}}{2} - t_1^-(z) = \frac{O_f + \gamma G_e z - \Omega_I}{R}, \end{aligned} \tag{6}$$

where $R = 2\gamma G_e L/t_1^{\max}$, and $\frac{t_1^{\max}}{2} = \frac{O_f - O_i}{R}$.

Since the durations of RF pulses on the spin packet at a specific position are relatively short, the spin evolutions during these periods are disregarded. After the first $\pi/2$ RF pulse, the density operator of I spin becomes

$$\sigma(0^+) = -I_y = -\frac{1}{2i}(I^+ - I^-). \tag{7}$$

For N-type COSY signals, the coherence-transfer pathway of this sequence is $0 \to +1 \to -1 \to +1 \to -1$, so we only need to follow the evolution of I^+ operator. During the $t_1^+(z)$ period, the spins evolve under chemical shifts, J-coupling, and gradient pulses. Just before the first π RF pulse, the density operator becomes

$$\sigma(t_1^+(z))^- = -\frac{1}{2i}\begin{bmatrix} I^+ e^{-i\Omega_I t_1^+(z)} e^{-i\gamma G_e z t_1^+(z)} \cos(\pi J_{IS} t_1^+(z)) \\ -2iI^+ S_z e^{-i\Omega_I t_1^+(z)} e^{-i\gamma G_e z t_1^+(z)} \sin(\pi J_{IS} t_1^+(z)) \end{bmatrix}. \tag{8}$$

The first π RF pulse turns the density operator into

$$\sigma(t_1^+(z))^+ = -\frac{1}{2i}\begin{bmatrix} I^- e^{-i\Omega_I t_1^+(z)} e^{-i\gamma G_e z t_1^+(z)} e^{2i\varphi_{rf}[t_1^+(z)]} \cos(\pi J_{IS} t_1^+(z)) \\ +2iI^- S_z e^{-i\Omega_I t_1^+(z)} e^{-i\gamma G_e z t_1^+(z)} e^{2i\varphi_{rf}[t_1^+(z)]} \sin(\pi J_{IS} t_1^+(z)) \end{bmatrix}, \tag{9}$$

where $\varphi_{rf}[t_1^+(z)]$ is the phase incrementation of the first π chirped pulse during the course of its sweep,

$$\varphi_{rf}[t_1^+(z)] = \int_0^{t_1^+(z)} O(t')dt' = O_i \cdot t_1^+(z) + \frac{1}{2} R \cdot (t_1^+(z))^2. \tag{10}$$

Before the second π RF pulse, we have

$$\begin{aligned} &\sigma\left(\frac{t_1^{\max}}{2} + t_1^-(z)\right)^- \\ &= -\frac{1}{2i}\begin{Bmatrix} I^- e^{i\Omega_I(-t_1^+(z)+\tau_1^+(z)+t_1^-(z))} e^{i\gamma G_e z(-t_1^+(z)+\tau_1^+(z)-t_1^-(z))} \\ \times e^{2i\varphi_{rf}[t_1^+(z)]} \cos[\pi J_{IS}(t_1^+(z) + \tau_1^+(z) + t_1^-(z))] \\ +2iI^- S_z e^{i\Omega_I(-t_1^+(z)+\tau_1^+(z)+t_1^-(z))} e^{i\gamma G_e z(-t_1^+(z)+\tau_1^+(z)-t_1^-(z))} \\ \times e^{2i\varphi_{rf}[t_1^+(z)]} \sin[\pi J_{IS}(t_1^+(z) + \tau_1^+(z) + t_1^-(z))] \end{Bmatrix}. \end{aligned} \tag{11}$$

The second π RF pulse turns the density operator into

$$\begin{aligned} &\sigma\left(\frac{t_1^{\max}}{2} + t_1^-(z)\right)^+ \\ &= -\frac{1}{2i}\begin{Bmatrix} I^+ e^{i\Omega_I(-t_1^+(z)+\tau_1^+(z)+t_1^-(z))} e^{i\gamma G_e z(-t_1^+(z)+\tau_1^+(z)-t_1^-(z))} \\ \times e^{2i(\varphi_{rf}[t_1^+(z)]-\varphi_{rf}[t_1^-(z)])} \cos[\pi J_{IS}(t_1^+(z) + \tau_1^+(z) + t_1^-(z))] \\ -2iI^+ S_z e^{i\Omega_I(-t_1^+(z)+\tau_1^+(z)+t_1^-(z))} e^{i\gamma G_e z(-t_1^+(z)+\tau_1^+(z)-t_1^-(z))} \\ \times e^{2i(\varphi_{rf}[t_1^+(z)]-\varphi_{rf}[t_1^-(z)])} \sin[\pi J_{IS}(t_1^+(z) + \tau_1^+(z) + t_1^-(z))] \end{Bmatrix}, \end{aligned} \tag{12}$$

where $\varphi_{rf}[t_1^-(z)]$ is the phase incrementation of the second π chirped pulse during the course of its sweep,

$$\varphi_{rf}[t_1^-(z)] = \int_0^{t_1^-(z)} O(t')dt' = O_i \cdot t_1^-(z) + \frac{1}{2} R \cdot (t_1^-(z))^2. \tag{13}$$

Before the second $\pi/2$ hard RF pulse, we have

$$\begin{aligned} &\sigma(t_1^{\max} + t_{\mathrm{mix}} + t_s)^- \\ &= -\frac{1}{2i}\begin{Bmatrix} I^+ e^{i\Omega_I(-t_1^+(z)+\tau_1^+(z)+t_1^-(z)-\tau_1^-(z))-i\Omega_I(t_{\mathrm{mix}}+t_s)} e^{i\gamma G_e z\left(-t_1^+(z)+\tau_1^+(z)-t_1^-(z)+\tau_1^-(z)\right)} \\ \times e^{2i\left(\varphi_{rf}[t_1^+(z)]-\varphi_{rf}[t_1^-(z)]\right)} \times e^{-i\gamma G_s z t_s} \cos\left[\pi J_{IS}(t_1^{\max} + t_{\mathrm{mix}} + t_s)\right] \\ -2iI^+ S_z e^{i\Omega_I\left(-t_1^+(z)+\tau_1^+(z)+t_1^-(z)-\tau_1^-(z)\right)-i\Omega_I(t_{\mathrm{mix}}+t_s)} e^{i\gamma G_e z\left(-t_1^+(z)+\tau_1^+(z)-t_1^-(z)+\tau_1^-(z)\right)} \\ \times e^{2i\left(\varphi_{rf}[t_1^+(z)]-\varphi_{rf}[t_1^-(z)]\right)} \times e^{-i\gamma G_s z t_s} \sin\left[\pi J_{IS}(t_1^{\max} + t_{\mathrm{mix}} + t_s)\right] \end{Bmatrix}. \end{aligned} \tag{14}$$

Introducing Eqs. (6), (10) and (13) into Eq. (14), we have

$$\begin{aligned} &\sigma(t_1^{\max} + t_{\mathrm{mix}} + t_s)^- \\ &= -\frac{1}{2i}\begin{Bmatrix} I^+ e^{-iCz\Omega_I - i\Omega_I(t_{\mathrm{mix}}+t_s)} \times e^{-i\gamma G_s z t_s} \cos\left[\pi J_{IS}(t_1^{\max} + t_{\mathrm{mix}} + t_s)\right] \\ -2iI^+ S_z e^{-iCz\Omega_I - i\Omega_I(t_{\mathrm{mix}}+t_s)} \times e^{-i\gamma G_s z t_s} \sin\left[\pi J_{IS}(t_1^{\max} + t_{\mathrm{mix}} + t_s)\right] \end{Bmatrix}, \end{aligned} \tag{15}$$

where C is a spatio-temporal encoding constant ($C = 2t_1^{\max}/L$).

After the successive action of the second $\pi/2$ hard RF pulse, the second G_s and G_p, the observable terms of the density operator become

$$\begin{aligned} &\sigma_{\mathrm{obs}}(t_1^{\max} + t_{\mathrm{mix}} + 2t_s + t_p)^+ \\ &= -\frac{1}{4i}\begin{Bmatrix} I^- \cos[\pi J_{IS}(t_1^{\max} + t_{\mathrm{mix}} + t_s)] \cos\left[\pi J_{IS}(t_s + t_p)\right] \times e^{i\Omega_I(t_s+t_p)} \\ +S^- \sin[\pi J_{IS}(t_1^{\max} + t_{\mathrm{mix}} + t_s)] \sin\left[\pi J_{IS}(t_s + t_p)\right] \times e^{i\Omega_S(t_s+t_p)} \end{Bmatrix} \cdot \\ &\quad \times e^{-iCz\Omega_I - i\Omega_I(t_{\mathrm{mix}}+t_s)} e^{i\gamma G_p z t_p} \end{aligned} \tag{16}$$

In the decoding period, spins evolve under chemical shifts, J-coupling and the gradient pulses. The observable terms of density operator become

$$\begin{aligned} &\sigma_{\mathrm{obs}}(t_1^{\max} + t_{\mathrm{mix}} + 2t_s + t_p + t_2) \\ &= -\frac{1}{4i}\begin{Bmatrix} I^- \cos\left[\pi J_{IS}(t_1^{\max} + t_{\mathrm{mix}} + t_s)\right] \cos\left[\pi J_{IS}(t_s + t_p + t_2)\right] \times e^{i\Omega_I(t_s+t_p+t_2)} \\ +S^- \sin\left[\pi J_{IS}(t_1^{\max} + t_{\mathrm{mix}} + t_s)\right] \sin\left[\pi J_{IS}(t_s + t_p + t_2)\right] \times e^{i\Omega_S(t_s+t_p+t_2)} \end{Bmatrix} \\ &\quad \times e^{-iCz\Omega_I - i\Omega_I(t_{\mathrm{mix}}+t_s)} e^{i\gamma G_p z t_p} e^{iz\cdot\int_0^{t_2}\gamma G_a(t)dt} \end{aligned} \tag{17}$$

Eq. (17) can be rewritten as

$$\sigma_{\mathrm{obs}}\left(t_1^{\max}+t_{\mathrm{mix}}+2t_s+t_p+t_2\right)=-\frac{1}{8i}\left\{\begin{array}{l} I^-\cos\left[\pi J_{IS}\left(t_1^{\max}+t_{\mathrm{mix}}+t_s\right)\right]e^{i\Omega_I t_2}e^{i\Omega_I(t_s+t_p)}\left[e^{i\pi J_{IS}(t_s+t_p+t_2)}+e^{-i\pi J_{IS}(t_s+t_p+t_2)}\right] \\ -iS^-\sin\left[\pi J_{IS}\left(t_1^{\max}+t_{\mathrm{mix}}+t_s\right)\right]e^{i\Omega_S t_2}e^{i\Omega_S(t_s+t_p)}\left[e^{i\pi J_{IS}(t_s+t_p+t_2)}-e^{-i\pi J_{IS}(t_s+t_p+t_2)}\right]\end{array}\right\} \times e^{-iCz\Omega_I-i\Omega_I(t_{\mathrm{mix}}+t_s)}e^{i\gamma G_p z t_p}e^{iz\cdot\int_0^{t_2}\gamma G_a(t)dt}. \tag{18}$$

So the resulting signals are

$$\begin{aligned} M_+(t_2,z)&=2^{-N}\times 4M_0\times\left\{Tr\left[\sigma_{\mathrm{obs}}\left(t_1^{\max}+t_{\mathrm{mix}}+2t_s+t_p+t_2\right)\left(I^++S^+\right)\right]\right\} \\ &=\frac{iM_0}{2}\times\left\{\begin{array}{l}\cos\left[\pi J_{IS}\left(t_1^{\max}+t_{\mathrm{mix}}+t_s\right)\right]e^{i\Omega_I t_2}e^{i\Omega_I\left(t_s+t_p\right)}\left[e^{i\pi J_{IS}(t_s+t_p+t_2)}+e^{-i\pi J_{IS}(t_s+t_p+t_2)}\right] \\ -i\sin\left[\pi J_{IS}\left(t_1^{\max}+t_{\mathrm{mix}}+t_s\right)\right]e^{i\Omega_S t_2}e^{i\Omega_S(t_s+t_p)}\left[e^{i\pi J_{IS}(t_s+t_p+t_2)}-e^{-i\pi J_{IS}(t_s+t_p+t_2)}\right]\end{array}\right\} \\ &\quad\times e^{-iCz\Omega_I-i\Omega_I(t_{\mathrm{mix}}+t_s)}e^{i\gamma G_p z t_p}e^{iz\cdot\int_0^{t_2}\gamma G_a(t)dt}, \end{aligned} \tag{19}$$

where M_0 is the equilibrium magnetization per unit volume of I or S spin (for the AX system, they are equal to each other), and N is the number of I or S spin in the sample.

From Eq. (19), we can see that echoes will form whenever $C\Omega_I=\gamma(\int_0^{t_2}G_a(t)dt+G_pt_p)$. The variation of G_pt_p will change the echo time during the decoding period, thus adjusting the locations of peaks in the indirect dimension and making them detectable. Processing the signals according to Eqs. (3) and (4) will give 2D frequency-domain signals. The first two terms in Eq. (19) represent the diagonal peaks of I spin, and the last two terms represent the cross peaks between I and S spins. The diagonal peak appears at $(\Omega_I,\Omega_I+\pi J_{IS})$ and $(\Omega_I,\Omega_I-\pi J_{IS})$, and the cross peak appears at $(\Omega_I,\Omega_S+\pi J_{IS})$ and $(\Omega_I,\Omega_S-\pi J_{IS})$. The central frequencies of the diagonal and cross peaks are (Ω_I,Ω_I) and (Ω_I,Ω_S), respectively. Similar deduction can be performed for S spin, and the resulting central frequencies are (Ω_S,Ω_I) and (Ω_S,Ω_S). Therefore, the sequence will yield a 2D COSY spectrum. According to Eq. (19), there is no J-splitting in the indirect dimension, i.e. homonuclear decoupling is obtained in this dimension, which is consistent with the conclusion mentioned by Giraudeau and Akoka [29]. Moreover, the variation of t_{mix} value will alter the relative signal intensities between diagonal and cross peaks. Due to various J-coupling constants in complex spin systems, the value of $\cos[\pi J_{IS}(t_1^{\max}+t_{\mathrm{mix}}+t_s)]$ or $\sin[\pi J_{IS}(t_1^{\max}+t_{\mathrm{mix}}+t_s)]$ for a specific J_{IS} may happen to be zero. Therefore, different t_{mix} values must be tested to avoid missing spectral peaks and have compromised signal intensities.

In consideration of the better performances when the encoding gradient of π chirped pulse is negative [30], the action of the phase-modulated encoding module of Fig. 1b on the spin packet at position z can be approximated by Fig. 2b. In combination with the EPI detection block, when condition $G_e^{(\pi/2)}t_{1,\max}^{(\pi/2)}+2G_e^{(\pi)}t_{1,\max}^{(\pi)}=0$ is set for the indirect-dimension encoding, the resulting signals for the I spin can be similarly deduced to be [24,30]

$$M_+(t_2,z)=-\frac{iM_0}{4}\left\{\begin{array}{l}\left[e^{i\pi J_{IS}\tau_1^{\pi/2}(z)}e^{i\pi J_{IS}(t_{1,\max}^{(\pi)}+t_{\mathrm{mix}}+t_s)}+e^{-i\pi J_{IS}\tau_1^{\pi/2}(z)}e^{-i\pi J_{IS}(t_{1,\max}^{(\pi)}+t_{\mathrm{mix}}+t_s)}\right]e^{i\Omega_I t_2}e^{i\Omega_I(t_s+t_p)}\left[e^{i\pi J_{IS}(t_s+t_p+t_2)}+e^{-i\pi J_{IS}(t_s+t_p+t_2)}\right] \\ -\left[e^{i\pi J_{IS}\tau_1^{\pi/2}(z)}e^{i\pi J_{IS}(t_{1,\max}^{(\pi)}+t_{\mathrm{mix}}+t_s)}-e^{-i\pi J_{IS}\tau_1^{\pi/2}(z)}e^{-i\pi J_{IS}(t_{1,\max}^{(\pi)}+t_{\mathrm{mix}}+t_s)}\right]e^{i\Omega_S t_2}e^{i\Omega_S(t_s+t_p)}\left[e^{i\pi J_{IS}(t_s+t_p+t_2)}-e^{-i\pi J_{IS}(t_s+t_p+t_2)}\right]\end{array}\right\} \times e^{-i[(B+C\Omega_I)\cdot z+D]-i\Omega_I(t_{\mathrm{mix}}+t_s)}e^{i\gamma G_p z t_p}e^{iz\cdot\int_0^{t_2}\gamma G_a(t)dt} \tag{20}$$

where $C=\frac{t_{1,\max}^{(\pi/2)}}{L}(1-\frac{G_e^{(\pi/2)}}{G_e^{(\pi)}})$ is a spatio-temporal encoding constant, $B=-\frac{\gamma G_e^{(\pi/2)}t_{1,\max}^{(\pi/2)}}{2}$, $D=-\frac{t_{1,\max}^{(\pi/2)}}{2}\{\Omega_I-\frac{(\Omega_I)^2}{\gamma G_e^{(\pi/2)}L}[1-(\frac{G_e^{(\pi/2)}}{G_e^{(\pi)}})^2]\}$ and $\tau_1^{(\pi/2)}(z)=(\frac{L-2z}{2L}-\frac{\Omega_I}{\gamma G_e^{(\pi/2)}L})t_{1,\max}^{(\pi/2)}$.

From Eq. (20) we can see that the conditions for echo formation are $B+C\Omega_I=\gamma(\int_0^{t_2}G_a(t)dt+G_pt_p)-\frac{t_{1,\max}^{(\pi/2)}}{L}\pi J_{IS}$ and $B+C\Omega_I=\gamma(\int_0^{t_2}G_a(t)dt+G_pt_p)+\frac{t_{1,\max}^{(\pi/2)}}{L}\pi J_{IS}$. Processing the signals according to Eqs. (3) and (4) will give 2D frequency-domain signals. For the AX spin-1/2 system, a 2D COSY spectrum will be obtained. Compared to Eq. (19), Eq. (20) is much more complicated and the echo conditions need to be carefully fulfilled. Moreover, there is J-coupling splitting in t_1 dimension. When the J-splitting is unresolvable, this may lead to broader linewidth than that from the constant-time phase-modulated encoding counterpart, thus lowering the spectral resolution in t_1 dimension.

The ultrafast gDQF-COSY pulse sequence is shown in Fig. 1d. It shares the same encoding module as the constant-time phase-modulated spatial encoding scheme. A π hard pulse and a $\pi/2$ hard pulse follow this encoding block before the EPI detection period. The π hard pulse is mainly used to reduce the signal attenuation. To achieve double-quantum filter, the last $\pi/2$ hard pulse is flanked by a pair of pulsed field gradients with a strength ratio of 1: -2 through the same duration. A purging gradient is also needed to localize the peak positions in the indirect dimension. The action of this pulse sequence on the spin packet at position z can be described as Fig. 2c, and the desired coherence-transfer pathway ($0\rightarrow+1\rightarrow-1\rightarrow+1\rightarrow+2\rightarrow-2\rightarrow-1$) is illustrated on the bottom. The spin evolution before the second $\pi/2$ hard RF pulse is the same as Eq. (15) excluding the action of G_s. After the second $\pi/2$ hard RF pulse, only +2 coherence order will survive for detection. The resulting signals is deduced to be

$$\begin{aligned} M_+(t_2,z)&=-\frac{M_0}{8}\left[e^{i\Omega_I t_2}e^{i\Omega_I(t_s+t_p)}+e^{i\Omega_S t_2}e^{i\Omega_S(t_s+t_p)}\right] \\ &\quad\times\left[e^{i\pi J_{IS}(t_s+t_p+t_2)}-e^{-i\pi J_{IS}(t_s+t_p+t_2)}\right]\sin\left[\pi J_{IS}(t_1^{\max}+t_{\mathrm{mix}})\right] \\ &\quad\times e^{-iCz\Omega_I-i\Omega_I t_{\mathrm{mix}}}\times e^{i\gamma z G_p t_p}\times e^{iz\cdot\int_0^{t_2}\gamma G_a(t)dt} \end{aligned} \tag{21}$$

From Eq. (21), we can see that echoes will form whenever $C\Omega_I=\gamma(\int_0^{t_2}G_a(t)dt+G_pt_p)$, as in the case of constant-time phase-modulated encoding g-COSY. Processing the signals according to Eqs. (3) and (4) will give 2D frequency-domain signals. Similarly, there is no J-splitting in the indirect dimension [29]. The main dif-

ference of Eq. (21) from Eq. (19) is that the diagonal and cross peaks have same phase, which means that they can be adjusted to pure adsorption mode. Moreover, they have same J dependence in signal intensity. When there is no J-coupling, the signals will disappear. All these features are consistent with conventional DQF-COSY.

3. Materials and methods

All experiments were performed at 298 K on a Varian NMR System 500 MHz spectrometer using a 5 mm ^{1}H $\{^{15}$N–^{31}P$\}$ indirect detection probe equipped with 3D gradient coils. A sample of propyl alcohol ($CH_3CH_2CH_2OH$) in $CDCl_3$ was used to test the capability of the pulse sequence shown in Fig. 1c for 2D COSY spectrum. The sample was prepared by adding 8 μl propyl alcohol to 992 μl $CDCl_3$ to form a 100 mmol l^{-1} solution. For comparison, a conventional ^{1}H–^{1}H 2D COSY spectrum was also acquired using the built-in g-COSY pulse sequence provided by Varian Inc. In the conventional g-COSY experiment, the duration of $\pi/2$ RF pulse was 11.75 μs, with the RF power of 58 dB. The pulse repetition time was 4 s. One hundred and twenty-eight points were acquired in the indirect dimension and the acquisition time t_2 was 300 ms. The spectral widths of the F1 and F2 dimensions were both 2000 Hz. The total acquisition time was about 10 min. In the constant-time phase-modulated encoding g-COSY experiment, the $\pi/2$ RF pulses were set the same as those used in conventional g-COSY experiment. The effective sample length was $L = 1.6$ cm. The π chirped pulses were created from the Pbox subroutine libraries at a digitization rate of 1.0 μs with an adiabatic coefficient of 1.2 to fulfill the adiabatic passage requirements. The gradient switching time was $\delta = 5$ μs. A delay (t_{mix}) of 15 ms was added after the second π chirped pulse to improve the coupling signals between different protons. The other relevant parameters were set as follows: $G_e = 15$ G/cm, $t_1^{max} = 40$ ms, $G_s = 1$ G/cm, $t_s = 2.5$ ms, $G_p = -10$ G/cm, $t_p = 0.28$ ms, $G_a = 30$ G/cm, $T_a = 200$ μs, and $N_2 = 80$. The total acquisition time was about 100 ms.

To compare our method (Fig. 1c) with the previous one (Fig. 1b), experiments on a sample of n-butylbromide/$CDCl_3$ solution were carried out. The sample was prepared by adding 12 μl n-butylbromide to 988 μl $CDCl_3$ to form a 100 mmol l^{-1} solution. The duration of $\pi/2$ RF pulse was 10.9 μs. The main experimental parameters are indicated in Fig. 3a and b. Other parameters and experimental conditions were set the same as those for propyl alcohol sample. The effective encoding time for Fig. 3a and b were both calculated to be 41.4 ms according to the expressions given by Giraudeau and Akoka [30]. The $\pi/2$ chirped pulse was created at a digitization rate of 1.0 μs with a adiabatic coefficient of 0.068 [31]. The same pair of field gradients were applied to flank the last $\pi/2$ hard pulse of both sequences in order to select the desired coherence order. Besides single scan, four-step phase cycling was also used to see its effect on the improvement of spectral quality. The pulse repetition time was 5 s. For the constant-time phase-modulated encoding sequence, the phases for the two $\pi/2$ hard pulses and the receiver were $(x, y, -x, -y)$, $(y, x, -y, -x)$ and $(-x, -y, x, y)$, respectively. For the real-time phase-modulated encoding sequence, the phases for the $\pi/2$ hard pulse and the receiver were $(x, y, -x, -y)$ and $(x, -x, x, -x)$, respectively.

The n-butylbromide/$CDCl_3$ sample was also used for 2D gDQF-COSY experiments. The main experimental parameters are indicated in Fig. 3c. Other parameters and experimental conditions were set the same as those for propyl alcohol sample. For comparison, experiments without and with a four-step phase cycling were performed. For the four-step phase cycling scheme, the three $\pi/2$ hard pulses in the sequence were all imposed for phase change. The phases for the three $\pi/2$ pulses were $(x, y, -x, -y)$, $(-x, -y, x, y)$ and $(y, -x, -y, x)$, respectively, and the receiver phase was $(y, -x, -y, x)$. The pulse repetition time was 5 s.

To obtain a frequency-domain spectrum, the acquired time-domain data points were first separated into two independent bidimensional data sets related to $+G_a$ and $-G_a$ periods, respectively, then both of them were zero-filled to a 100×100 (k, t_2) matrix before regular FT against t_2 for a 2D COSY spectrum. Combination of these two data sets results in an $\sqrt{2}$ improvement of the spectral sensitivity [19,20]. All the data were processed with the aid of our custom-written program with Matlab 7.7.0 (The Math Works Inc.).

4. Results and discussion

The experimental spectrum of the sample of propyl alcohol in $CDCl_3$ acquired using the constant-time phase-modulated encoding g-COSY pulse sequence is shown in Fig. 4a, together with the conventional 2D g-COSY spectrum shown in Fig. 4b. It reveals that the constant-time phase-modulated encoding g-COSY sequence does give a correct 2D ^{1}H–^{1}H COSY spectrum (Fig. 4a). Compared to Fig. 4b, the intensities of most cross peaks in Fig. 4a are weaker partly due to single scan. The lower spectral resolution is an intrinsic limitation of current ultrafast methods. If the encoding time (t_1^{max}) is elongated for a better spectral resolution in the indirect dimension, the spectrum will be severely deteriorated due to prominent effects of molecular diffusion [29,30,32]. Therefore, a compromised encoding time should be set to get a 2D COSY spectrum with acceptable resolution in a practical experiment. Nevertheless, all the chemical shift and J-coupling network information can still be obtained from Fig. 4a. Since the constant-time phase-modulated encoding experiment can be completed within much shorter time, it can be used in the cases where the experimental time is mainly concerned. For this sample, the total experimental time needed for a 2D COSY spectrum using our method is only about 100 ms, much shorter than the conventional 2D g-COSY counterpart (about 10 min).

The single-scan 2D ^{1}H–^{1}H COSY spectra of the sample of n-butylbromide/$CDCl_3$ acquired by using the constant-time phase-modulated encoding g-COSY method and real-time phase-modulated encoding g-COSY method are illustrated in Fig. 5, together with the initial parts of the time-domain signals. Both spectra, presented

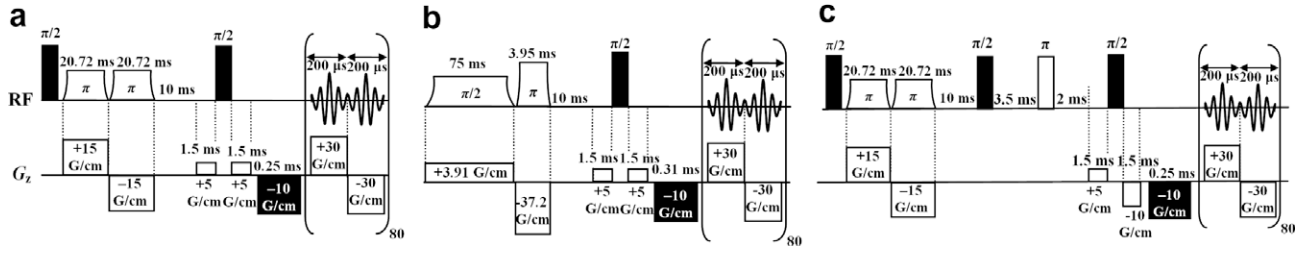

Fig. 3. Pulse sequences used for single-scan 2D ^{1}H–^{1}H COSY experiments of n-butylbromide/$CDCl_3$ sample with parameters indicated. (a) Constant-time phase-modulated encoding g-COSY sequence, (b) real-time phase-modulated encoding g-COSY sequence, and (c) constant-time phase-modulated encoding gDQF-COSY sequence.

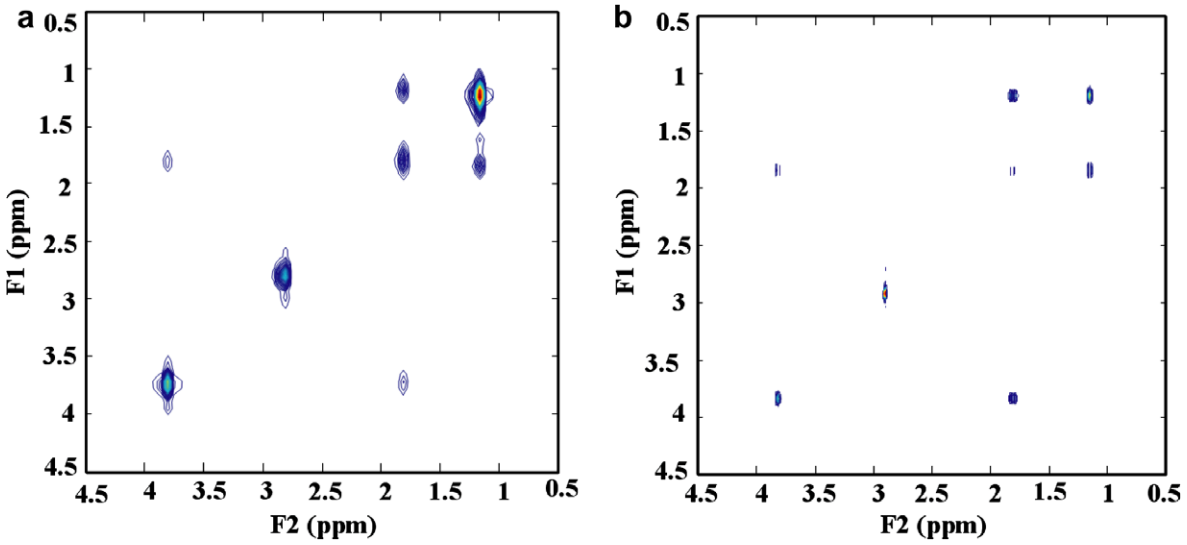

Fig. 4. Absolute-value ^{1}H–^{1}H g-COSY spectra of propyl alcohol in $CDCl_3$. (a) Single-scan spectrum acquired using the constant-time phase-modulated encoding pulse sequence shown in Fig. 1c within about 100 ms and (b) conventional spectrum acquired within about 10 min.

in magnitude mode, were processed with the same procedure and same post-processing parameters.

In order to impartially make these two methods comparable, we have carefully set the experimental parameters, especially the effective encoding time, so that the experiments were performed in the conditions as close as possible. The comparison between the two COSY spectra (Fig. 5a and b) indicates that both spectra have approximately identical resolution in the direct dimension due to the same decoding schemes. The half-height widths of the peak located at 1.3 ppm (the strongest peak) in the accumulated projection spectra (absolute-value mode) in the direct dimension are 24 and 27 Hz for constant-time phase-modulated encoding spectrum (Fig. 5a) and real-time phase-modulated encoding spectrum (Fig. 5b), respectively. Whereas the spectrum obtained with the constant-time phase-modulated encoding has much higher resolution in the indirect dimension. The half-height widths of the peak at 1.3 ppm in the accumulated projection spectra in the indirect dimension are 48 and 82 Hz, respectively, for these two encoding schemes. The higher resolution would benefit the application of ultrafast 2D COSY method on complex proton systems. The comparison between the time-domain signals shown in Fig. 5d and e indicates that the signal obtained with the constant-time phase-modulated encoding method has higher SNR than the counterpart obtained with the real-time phase-modulated encoding method. Four echoes can be clearly observed during each $+G_a$ or $-G_a$ sampling period as shown in Fig. 5d, whereas the echoes shown in Fig. 5e are not so clear due to serious noises. This conclusion is further confirmed by the SNR of the frequency-domain signals. The SNR of the peak at 1.3 ppm in the indirect dimension is approximately 95 for the constant-time phase-modulated encoding method and 61 for the real-time phase-modulated encoding method. The better results from the constant-time phase-modulated encoding method (higher resolution and SNR) may be mainly attributed to the more accurate excitation by the π–π chirped pulses than by $\pi/2$–π chirped pulses and the elimination of J-splitting for constant-time phase-modulated encoding method. All the spectral resolution and SNR data mentioned above are average values from five consecutive experiments performed with the same parameters. The spectral quality is improved after four-step phase cycling (Fig. 5g and h). For the peak at 1.3 ppm, the half-height width becomes 39 and 75 Hz, and the SNR becomes 127 and 85, respectively, in the indirect direction. Of course this improvement is at a cost of experimental time. The total experimental time increased to about 20 s for an acquisition with four-step phase cycling.

In practice, it is significant for an experiment to be performed rapidly and conveniently. In constant-time phase-modulated encoding 2D g-COSY experiment, instead of two different chirped pulses, two same π chirped pulses, together with a pair of reverse gradients ($+G_e$, $-G_e$) over equal time during the course of spin encoding are used. So the experiment is relatively easy to implement, without too much cumbersome parameter calibration work. By contrast, in the real-time phase-modulated encoding 2D g-COSY experiment, the conditions of $G_e^{(\pi/2)}t_{1,\max}^{(\pi/2)} = -2G_e^{(\pi)}t_{1,\max}^{(\pi)}$ and $G_e^{(\pi)} \approx 10G_e^{(\pi/2)}$ are chosen for the indirect-dimension encoding, and the $\pi/2$ and π chirped pulses should be set according to the relevant parameters ($G_e^{(\pi/2)}$, $G_e^{(\pi)}$, $t_{1,\max}^{(\pi/2)}$ and $t_{1,\max}^{(\pi)}$). Therefore, a longer time is needed to calibrate these parameters and generate the $\pi/2$ and π chirped pulses for a 2D COSY spectrum. Moreover, the result of real-time phase-modulated encoding experiment is more sensitive to experimental parameter variations, such as pulse power or frequency offset [32].

The single-scan 2D gDQF-COSY spectrum of the sample of *n*-butylbromide/$CDCl_3$ is shown in Fig. 5c. The experimental time for this spectrum is about 100 ms. This result demonstrates the feasibility of the ultrafast gDQF-COSY sequence. Compared to Fig. 5a, the signal intensity is weakened since DQF causes 50% signal loss. On the other hand, the intensities of cross peaks become more comparable to the intensities of diagonal peaks as a result of a relative suppression of diagonal peaks. For the peak at 1.3 ppm in the accumulated projection spectra, the half-height widths are 21 and 42 Hz in the direct and indirect direction, respectively. The SNR of the same peak is 87 in the indirect dimension. These values are close to the ones obtained from Fig. 5a. The four-step phase cycling improves the corresponding resolution and SNR in the indirect dimension to 19 Hz and 138, respectively (Fig. 5i), much better than the effect of phase cycling on the ultrafast g-COSY. Nevertheless, the present resolution is still not enough for a phase-sensitive COSY spectrum.

5. Conclusion

Ultrafast 2D NMR spectroscopy will largely save experimental time, thus it is an important research topic in NMR community.

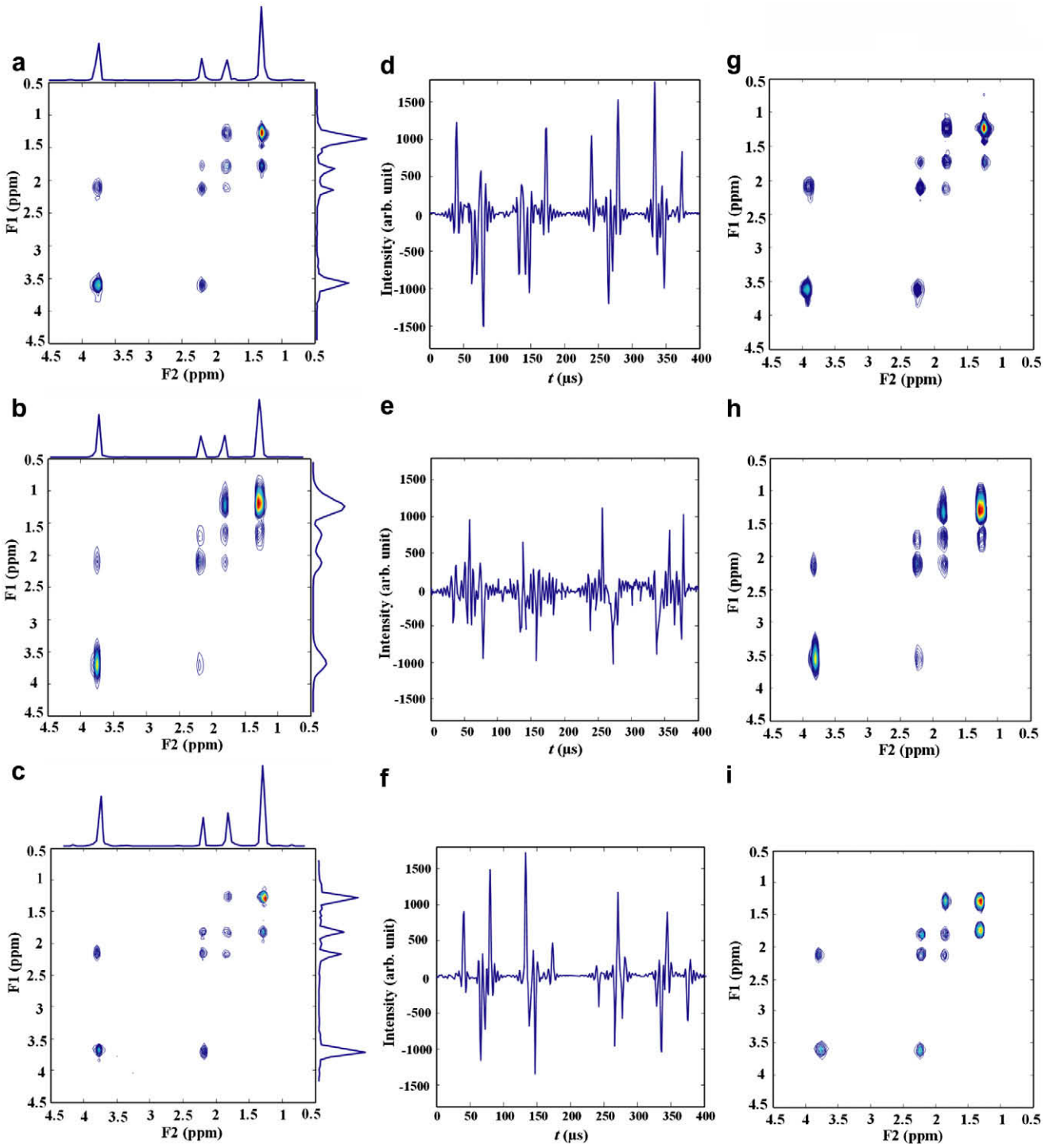

Fig. 5. Ultrafast 2D ^{1}H–^{1}H COSY spectra and corresponding time-domain signals in the first two decoding periods of the *n*-butylbromide/$CDCl_3$ sample. (a) Single-scan spectrum obtained using the constant-time phase-modulated encoding g-COSY pulse sequence shown in Fig. 3a, (b) single-scan spectrum obtained using the real-time phase-modulated encoding g-COSY pulse sequence shown in Fig. 3b, and (c) single-scan spectrum obtained using the constant-time phase-modulated encoding gDQF-COSY pulse sequence shown in Fig. 3c. All spectra were recorded within about 100 ms. Their accumulated projections in both direct and indirect dimensions are shown for comparison. (d–f) Time-domain signals corresponding to (a–c), respectively. (g–i) Spectra corresponding to (a–c), respectively, obtained with four-step phase cycling within about 20 s. All the spectra are displayed in absolute-value mode.

In this paper, ultrafast 2D g-COSY and gDQF-COSY methods were proposed based on constant-time phase-modulated encoding with a π–π chirped pulse scheme. With these methods, 2D COSY spectra can be obtained efficiently within sub-second. Compared to the previous real-time phase-modulated encoding method, our methods improve the spectral SNR and resolution in the indirect dimension. Furthermore, 2D COSY spectra can be obtained more easily due to simpler parameter setting and calibration. These advantages would make them more applicable in practical application.

Acknowledgments

The authors are grateful to Prof. Lucio Frydman and Dr. Assaf Tal (Weizmann Institute of Science, Israel) for assistance during the

course of this study. This work was supported by the NNSF of China under Grants 10875101 and 10774125, the Key Project of Chinese Ministry of Education under Grant 109092, and National Key Technology R&D Program of China (2006BAK03A22).

References

[1] D.M. Grant, R.K. Harris, Encyclopedia of NMR, John Wiley & Sons Ltd., Chichester, 1996.
[2] J. Jeener, Lecture at International Ampere Summer School, Basko Polje, Yugoslavia, 1971.
[3] W.P. Aue, E. Bartholdi, R.R. Ernst, Two-dimensional spectroscopy-application to nuclear magnetic resonance, J. Chem. Phys. 64 (1976) 2229–2246.
[4] U. Piantini, O.W. Sorensen, R.R. Ernst, Multiple quantum filters for elucidating NMR coupling networks, J. Magn. Reson. 104 (1982) 6800–6801.
[5] A.J. Shaka, R. Freeman, Simplification of NMR spectra by filtration through multiple-quantum coherence, J. Magn. Reson. 51 (1983) 169–193.
[6] M. Rance, O.W. Sorensen, G. Bodenhausen, G. Wagner, R.R. Ernst, K. Wutahrich, Improved spectral resolution in COSY ^{1}H NMR spectra of proteins via double quantum filtering, Biochem. Biophys. Res. Commun. 117 (1983) 479–485.
[7] P. Schanda, B. Brutscher, Very fast two-dimensional NMR spectroscopy for real-time investigation of dynamic events in proteins on the time scale of seconds, J. Am. Chem. Soc. 127 (2005) 8014–8015.
[8] E. Kupce, R. Freeman, Fast multidimensional NMR: radial sampling of evolution space, J. Magn. Reson. 173 (2005) 317–321.
[9] B.E. Coggins, P. Zhou, Polar Fourier transforms of radially sampled NMR data, J. Magn. Reson. 182 (2006) 84–95.
[10] B.E. Coggins, P. Zhou, Sampling of the NMR time domain along concentric rings, J. Magn. Reson. 184 (2007) 207–221.
[11] B.E. Coggins, P. Zhou, High resolution 4-D spectroscopy with sparse concentric shell sampling and FFT-CLEAN, J. Biomol. NMR 42 (2008) 225–239.
[12] H. Barkhuijsen, D.R. Beer, V.D. Ormondt, W.M.M.J. Bovée, Retrieval of frequencies, amplitudes, damping factors, and phases from time-domain signals using a linear least-squares procedure, J. Magn. Reson. 61 (1985) 465–481.
[13] A.S. Stern, K.B. Li, J.C. Hoch, Modern spectrum analysis in multidimensional NMR spectroscopy: comparison of linear-prediction extrapolation and maximum-entropy reconstruction, J. Am. Chem. Soc. 124 (2002) 1982–1993.
[14] J.C. Hoch, Maximum entropy signal processing of two-dimensional NMR data, J. Magn. Reson. 64 (1985) 436–440.
[15] E. Kupce, R. Freeman, Projection-reconstruction technique for speeding up multidimensional NMR spectroscopy, J. Am. Chem. Soc. 126 (2004) 6429–6440.
[16] V.A. Mandelshtam, H.S. Taylor, A.J. Shaka, Application of the filter diagonalization method to one- and two-dimensional NMR spectra, J. Magn. Reson. 133 (1998) 304–312.
[17] E. Kupce, R. Freeman, Frequency-domain Hadamard spectroscopy, J. Magn. Reson. 162 (2003) 158–165.
[18] E. Kupce, R. Freeman, Two-dimensional Hadamard spectroscopy, J. Magn. Reson. 162 (2003) 300–310.
[19] L. Frydman, A. Lupulescu, T. Scherf, Principles and features of single-scan two-dimensional NMR spectroscopy, J. Am. Chem. Soc. 125 (2003) 9204–9217.
[20] L. Frydman, T. Scherf, A. Lupulescu, The acquisition of multidimensional NMR spectra within a single scan, Proc. Natl. Acad. Sci. USA 99 (2002) 15858–15862.
[21] Y. Shrot, L. Frydman, Ghost-peak suppression in ultrafast two-dimensional NMR spectroscopy, J. Magn. Reson. 164 (2003) 351–357.
[22] P. Pelupessy, Adiabatic single scan two-dimensional NMR spectroscopy, J. Am. Chem. Soc. 125 (2003) 12345–12350.
[23] Y. Shrot, B. Shapira, L. Frydman, Ultrafast 2D NMR spectroscopy using a continuous spatial encoding of the spin interactions, J. Magn. Reson. 171 (2004) 163–170.
[24] A. Tal, B. Shapira, L. Frydman, A continuous phase-modulated approach to spatial encoding in ultrafast 2D NMR spectroscopy, J. Magn. Reson. 176 (2005) 107–114.
[25] P. Giraudeau, S. Akoka, A new detection scheme for ultrafast 2D *J*-resolved spectroscopy, J. Magn. Reson. 186 (2007) 352–357.
[26] N.S. Andersen, W. Kockenberger, A simple approach for phase-modulated single-scan 2D NMR spectroscopy, Magn. Reson. Chem. 43 (2005) 795–797.
[27] Y. Shrot, L. Frydman, Spatial encoding strategies for ultrafast multidimensional nuclear magnetic resonance, J. Chem. Phys. 128 (2008) 052209.
[28] P. Pelupessy, E. Rennella, G. Bodenhausen, High-resolution NMR in magnetic fields with unknown spatiotemporal variations, Science 324 (2009) 1693–1697.
[29] P. Giraudeau, S. Akoka, Sources of sensitivity losses in ultrafast 2D NMR, J. Magn. Reson. 192 (2008) 151–158.
[30] P. Giraudeau, S. Akoka, Resolution and sensitivity aspects of ultrafast *J*-resolved 2D NMR spectra, J. Magn. Reson. 190 (2008) 339–345.
[31] Y. Shrot, L. Frydman, Spatially encoded NMR and the acquisition of 2D magnetic resonance images within a single scan, J. Magn. Reson. 172 (2005) 179–190.
[32] P. Giraudeau, S. Akoka, Sensitivity losses and line shape modifications due to molecular diffusion in continuous encoding ultrafast 2D NMR experiments, J. Magn. Reson. 195 (2008) 9–16.